

Color dipole cross section in the DGLAP improved saturation model

G.R.Boroun*

Physics Department, Razi University, Kermanshah 67149, Iran

(Dated: May 11, 2022)

We show that the geometric scaling of the dipole cross section can be explained using standard DGLAP perturbative evolution. The DGLAP improved saturation model due to the Laplace transforms method is considered at LO and NNLO approximations from the experimental data by relying on a Froissart-bounded parametrization of $F_2(x, Q^2)$. These results are comparable with Golec-Biernat-Wüsthoff (GBW) model in a wide kinematic region rQ_s which takes into account charm mass. The successful description of $\sigma_{\text{dip}}(x, r)/\sigma_0$ and $\sigma_{\text{dip}}(rQ_s)/\sigma_0$ are presented.

1. Introduction

Recently an update [1] on the saturation model of deep inelastic scattering (DIS) by Golec-Biernat *et al.* is presented by introducing the results of new fits [2] to the extracted HERA data [3] on the proton structure function at small x with the GBW saturation model and its modification to cover high values of Q^2 . When $x \ll 1$, the DGLAP [4] or the BFKL [5] evolution equations predict that the small x structure of the proton is dominated by a strongly rising gluon density, which drives a similar rise of the sea quark densities. In this region gluons in the proton form a dense system with mutual interaction and recombination which leads to the saturation of the total cross section [5]. For $x \approx Q^2/W^2 \ll 1$, the virtual spacelike photon on the proton fluctuates are defined into on-shell quark-antiquark, $q\bar{q}$, vector state. Here Q^2 refers to the photon virtuality and W to the photon-proton center-of-mass energy. In this process photon interact with the proton via coupling of two gluons to the $q\bar{q}$ color dipole, where this called the color dipole model (CDM). The mass of $q\bar{q}$ dipole, in terms of the transverse momentum \vec{k}_\perp is given by $M_{q\bar{q}}^2 = \frac{\vec{k}_\perp^2}{z(1-z)}$, where \vec{k}_\perp is defined with respect to the photon direction and the variable z characterizes the distribution of the momenta between quark and antiquark [6]. The lifetime of the $q\bar{q}$ dipole is defined by $\tau = \frac{W^2}{Q^2 + M_{q\bar{q}}^2} \gg \frac{1}{M_p}$, which it is much longer than its typical interaction time with the target at small x . This condition not only restricts the kinematical range of the color dipole model to $x \ll 1$ but also saturate the γ^* -proton cross section with $x < 0.1$ [7].

Some years ago [8] the saturation model was shown by Golec-Biernat and Wüsthoff which give an elegant and accurate account of DIS at small x and has been formulated to new models in recent years [9-13]. This type saturation occurs when the photon wavelength $1/Q$ reaches the size of the proton. It is well known that the dipole

picture is a factorization scheme for DIS, which is particularly convenient for the inclusion of unitarity corrections at small x . In the mixed representation, the scattering between the virtual photon γ^* and the proton is seen as the color dipole where the transverse dipole size r and the longitudinal momentum fraction z with respect to the photon momentum are defined. The amplitude for the complete process is simply the produce of these subprocess amplitudes, as the DIS cross section is factorized into a light-cone wave function and a dipole cross section. Using the optical theorem, this leads to the following expression for the γ^*p cross-sections

$$\sigma_{L,T}^{\gamma^*p}(x, Q^2) = \int dz d^2\mathbf{r} |\Psi_{L,T}(\mathbf{r}, z, Q^2)|^2 \sigma_{\text{dipole}}(\tilde{x}_f, \mathbf{r}), \quad (1)$$

and the F_2 structure function is defined as

$$F_2(x, Q^2) = \frac{Q^2}{4\pi^2\alpha} [\sigma_L^{\gamma^*p}(x, Q^2) + \sigma_T^{\gamma^*p}(x, Q^2)]. \quad (2)$$

The subscript L and T referring to the transverse and longitudinal polarization state of the exchanged boson. Here $\Psi_{L,T}$ are the appropriate spin averaged light-cone wave functions of the photon and $\sigma_{\text{dip}}(\tilde{x}_f, r)$ is the dipole cross-section which related to the imaginary part of the $(q\bar{q})p$ forward scattering amplitude and $\tilde{x}_f \equiv x(1 + 4m_f^2/Q^2)$ is equivalent to the Bjorken variable and provides an interpolation for the $Q^2 \rightarrow 0$ limit, m_f is the mass of the quark of flavour f . The variable z , with $0 \leq z \leq 1$, characterizes the distribution of the momenta between quark and antiquark. The square of the photon wave function describes the probability for the occurrence of a $(q\bar{q})$ fluctuation of transverse size with respect to the photon polarization [1,8-15].

The dipole hadron cross section σ_{dip} contains all information about the target and the strong interaction physics. There are several phenomenological implementations for this quantity and the main feature is to be able to match the soft (low Q^2) and hard (large Q^2) regimes in an unified way. In Ref.[8], the dipole cross section was proposed to have the eikonal-like form

$$\sigma_{\text{dip}}(\tilde{x}_f, r) = \sigma_0(1 - e^{-r^2 Q_s^2/4}), \quad (3)$$

*Electronic address: grboroun@gmail.com; boroun@razi.ac.ir

where $Q_s(\tilde{x})$ plays the role of the saturation momentum, parametrized as $Q_s^2(x) = Q_0^2(\tilde{x}/x_0)^{-\lambda}$. Parameters Q_0 and x_0 set dimension and absolute value of the saturation scale and exponent λ governs x behavior of Q_s^2 . The saturation (non-linear QCD) is energy dependent and marks the transition between the linear (leading twist) perturbative QCD regime and saturation domain. The resulting dipole cross section presents the colour transparency property, i.e. $\sigma_{\text{dip}} \sim r^2$ when $r \rightarrow 0$, which is purely pQCD phenomenon and the saturation property, i.e. $\sigma_{\text{dip}} \sim \sigma_0$ at large r , which imposes the unitarity condition. The GBW model was updated in [10,16] to improve the large Q^2 description of F_2 by a modification of the small r behavior of the dipole cross section to include the DGLAP evolved gluon distribution. A similar in spirit parameterization of the dipole scattering amplitude, based on the Balitsky-Kovchegov (BK) equation solution, was proposed in [9]. The BK equation [17] for a dipole scattering amplitude was proposed in terms of the hierarchy of equations for Wilson line operators in the limit of large number of colors N_c . The geometrical scaling (GS) [18] at the high-energy limit of perturbative QCD obtained from the BK equation [17] and the Colour Glass Condensate (CGC) formalism [19]. Geometrical scaling is connected to the existence of the saturation scale and is defined as dependence of the dipole cross section only on one dimensionless variable. In the limit of large Q^2 values, the structure function (2) does not exactly match with the DGLAP formula for F_2 , i.e. the saturation model does not include logarithmic scaling violations. Since the energy dependence in large Q^2 region is mainly due to the behavior of the dipole cross section at small dipole size r , therefore authors in Ref.[10] investigated the DGLAP evolution for small dipoles. Bartels-Golec-Bienat-Kowalski (BGBK) improved the dipole cross section by adding the collinear DGLAP effects. Indeed the BGBK model is the implementation of QCD evolution in the the dipole cross section which depends on the gluon distribution. The following modification of the DGLAP improved saturation model [1] proposed for the dipole cross section as

$$\sigma_{\text{dip}} = \sigma_0 \left\{ 1 - \exp\left(-\frac{\pi^2 r^2 \alpha_s(\mu^2) G(\tilde{x}, \mu^2)}{3\sigma_0}\right) \right\}, \quad (4)$$

where the hard scale is assumed to have the form

$$\mu^2 = C/r^2 + \mu_0^2, \quad (5)$$

and the parameters C and μ_0^2 are obtained from the fit to the DIS data [1]. The gluon distribution $G(x, \mu^2)$ obeys the DGLAP evolution equation truncated to the gluonic sector, as reported in literatures [1,8-19], by the following form

$$\frac{\partial g(x, \mu^2)}{\partial \ln \mu^2} = \frac{\alpha_s(\mu^2)}{2\pi} \int_x^1 \frac{dz}{z} P_{gg}(z) g\left(\frac{x}{z}, \mu^2\right), \quad (6)$$

where $g(x, \mu^2)$ is the gluon density and $G(x, \mu^2) = xg(x, \mu^2)$. The splitting function P_{gg} at the leading-order (LO) approximation reads

$$P_{gg}^{\text{LO}}(z) = 2C_A \left(\frac{z}{(1-z)_+} + \frac{(1-z)}{z} + z(1-z) \right) + \delta(1-z) \frac{(11C_A - 4n_f T_R)}{6}, \quad (7)$$

with $C_A = N_c = 3$, $C_F = \frac{N_c^2 - 1}{2N_c} = \frac{4}{3}$ and $T_f = \frac{1}{2}n_f$ where n_f is the active quark flavor. The convolution integrals in (6) which contains plus prescription, $()_+$, can be easily calculate by

$$\int_x^1 \frac{dy}{y} f\left(\frac{x}{y}\right)_+ g(y) = \int_x^1 \frac{dy}{y} f\left(\frac{x}{y}\right) [g(y) - \frac{x}{y} g(x)] - g(x) \int_0^x f(y) dy. \quad (8)$$

The initial gluon distribution is defined at the scale μ_0^2 in the form [1]

$$xg(x, \mu_0^2) = A_g x^{-\lambda_g} (1-x)^{5.6}. \quad (9)$$

The choice of the power 5.6, which regulates the large- x behavior, and another parameters (i.e., A_g and λ_g) are motivated by global fits to DIS data with the LO DGLAP equation in literatures.

Although BGBK model is successful in describing dipole cross section at large values of r as the two models (GBW and BGBK) overlap in this region but they differ in the small r region where the running of the gluon distribution starts to play a significant role. Indeed the DGLAP improved model of σ_{dip} significantly improves agreement at large values of Q^2 without affecting the physics of saturation responsible for transition to small Q^2 . As expected, GS is true for the DGLAP improved model curve for the scaling variable $rQ_s \geq 1$ and for the GBW model curve for the whole region [1].

It is well known that the color dipole cross sections determined from the original structure functions with a parametrization of the deep inelastic structure function for electromagnetic scattering with protons in Ref.[20]. The authors in Ref.[20] presented the dipole cross section from an approximate form of the presumed dipole cross section convoluted with the perturbative photon wave function for virtual photon splitting into a color dipole with massless quarks. Some approximated analytical solutions in color dipole model, have been reported in last years [21,22] with considerable phenomenological success. The analytical methods of the unpolarized DGLAP evolution equations have been discussed considerably in Mellin and Laplace transformation [23,24]. We present a modification of the DGLAP improved saturation model, with respect to the Laplace transform technique by employing the parametrization of proton

structure function at leading-order up to next-to-next-to-leading order (NNLO) approximations, which preserves its behavior success in the low and high Q^2 regions. We show that GS holds for the DGLAP improved model in a wide kinematic region rQ_s . In next section, we introduce the theoretical details of the model due to the Laplace transform technique and discuss its qualitative features. We then derive the dipole cross section with respect to the parametrization of F_2 at LO up to NNLO approximations. In Section 3 we describe our results and discuss their physical implications in comparison with the GBW model. Section 4 contains conclusions.

2. The Model

An analytical expression for $F_2(x, Q^2)$ has suggested by authors in Ref. [25] which describes fairly well the available experimental data on the reduced cross section in full accordance with the Froissart predictions [26]. This parameterization provides reliable structure function $F_2(x, Q^2)$ according to a combined fit of the H1 and ZEUS Collaborations data [27] in a range of the kinematical variables x and Q^2 , $x \leq 0.1$ and $0.15 \text{ GeV}^2 < Q^2 < 3000 \text{ GeV}^2$, as

$$F_2(x, Q^2) = D(Q^2)(1-x)^n \sum_{m=0}^2 A_m(Q^2) L^m, \quad (10)$$

and can be applied as well in analyses of ultra-high energy processes with cosmic neutrinos. The effective parameters are defined by the following forms

$$D(Q^2) = \frac{Q^2(Q^2 + \lambda M^2)}{(Q^2 + M^2)^2}, \quad A_0(Q^2) = a_{00} + a_{01} L_2, \\ A_i(Q^2) = \sum_{k=0}^2 a_{ik} L_2^k, \quad i = (1, 2), \quad (11)$$

with the logarithmic terms L as

$$L = \ln \frac{1}{x} + L_1, \quad L_1 = \ln \left(\frac{Q^2}{Q^2 + \mu^2} \right), \\ L_2 = \ln \left(\frac{Q^2 + \mu^2}{Q^2} \right), \quad (12)$$

where the effective parameters M and μ^2 are the effective mass and a scale factor, respectively. The additional parameters with their statistical errors are given in Table I. According to the DGLAP Q^2 -evolution equation, the singlet and gluon distribution functions are related by the following form

$$\frac{\partial F_2(x, Q^2)}{\partial \ln Q^2} = -\frac{a_s(Q^2)}{2} [P_{qq}(x) \otimes F_2(x, Q^2) \\ + \langle e^2 \rangle P_{qg}(x) \otimes xg(x, Q^2)], \quad (13)$$

where

$$P_{a,b}(x) = P_{a,b}^{(0)}(x) + a_s(Q^2) \tilde{P}_{a,b}^{(1)}(x) + a_s^2(Q^2) \tilde{P}_{a,b}^{(2)}(x) \quad (14)$$

and

$$\tilde{P}_{ab}^{(n)}(x) = P_{ab}^{(n)}(x) + [C_{2,s} + C_{2,g} + \dots] \otimes P_{ab}^{(0)}(x) + \dots$$

The quantities \tilde{P}_{ab} 's are expressed via the known splitting and Wilson coefficient functions in the literatures [28,29] and $a_s(Q^2) = \alpha_s(Q^2)/4\pi$.

One can substantially simplify the calculations by considering Eq.(13) in the space of Laplace transform techniques, and taking advantage of the fact the convolution form $f_1(x) \otimes f_2(x)$ in x space becomes merely a product of individual Laplace transforms of the corresponding functions in the Laplace space. By considering the variable definitions $v \equiv \ln(1/x)$ and $w \equiv \ln(1/z)$, Eq.(13) reads as

$$\frac{\partial \hat{\mathcal{F}}_2(v, Q^2)}{\partial \ln Q^2} = \int_0^v [\hat{\mathcal{F}}_2(v, Q^2) \hat{\mathcal{H}}_{2,s}^{(\varphi)}(a_s(Q^2), v-w) \\ + \langle e^2 \rangle \hat{\mathcal{G}}(v, Q^2) \hat{\mathcal{H}}_{2,g}^{(\varphi)}(a_s(Q^2), v-w)] dw, \quad (15)$$

where

$$\frac{\partial \hat{\mathcal{F}}_2(v, Q^2)}{\partial \ln Q^2} \equiv \frac{\partial F_2(e^{-v}, Q^2)}{\partial \ln Q^2}, \\ \hat{\mathcal{G}}(v, Q^2) \equiv G(e^{-v}, Q^2), \\ \hat{\mathcal{H}}^{(\varphi)}(a_s(Q^2), v) \equiv e^{-v} \hat{P}_{a,b}^{(\varphi)}(a_s(Q^2), v).$$

Here ϕ denotes the order in running coupling $\alpha_s(Q^2)$ and

$$P_{a,b}^{(\varphi)}(a_s, x) = \sum_{\phi=0}^{\varphi} a_s^{\phi+1}(Q^2) P_{a,b}^{(\phi)}(x).$$

The Laplace transform of $\hat{\mathcal{H}}(a_s(Q^2), v)$'s are given by the following forms

$$\Phi_f^{(\varphi)}(a_s(Q^2), s) \equiv \mathcal{L}[\hat{\mathcal{H}}_{2,s}^{(\varphi)}(a_s(Q^2), v); s] \\ = \int_0^\infty \hat{\mathcal{H}}_{2,s}^{(\varphi)}(a_s(Q^2), v) e^{-sv} dv, \\ \Theta_f^{(\varphi)}(a_s(Q^2), s) \equiv \mathcal{L}[\hat{\mathcal{H}}_{2,g}^{(\varphi)}(a_s(Q^2), v); s] \\ = \int_0^\infty \hat{\mathcal{H}}_{2,g}^{(\varphi)}(a_s(Q^2), v) e^{-sv} dv.$$

We know that the Laplace transforms of the convolution factors are simply the ordinary products of the Laplace transforms of the factors. Therefore, Eq.(15) in the Laplace space s reads as

$$\frac{\partial f_2(s, Q^2)}{\partial \ln Q^2} = \Phi_f^{(\varphi)}(a_s(Q^2), s) f_2(s, Q^2) \\ + \langle e^2 \rangle \Theta_f^{(\varphi)}(a_s(Q^2), s) g(s, Q^2), \quad (16)$$

where

$$\begin{aligned}\mathcal{L}[\widehat{\mathcal{F}}_2(v, Q^2); s] &= f_2(s, Q^2), \\ \mathcal{L}[\widehat{\mathcal{G}}(v, Q^2); s] &= g(s, Q^2).\end{aligned}$$

The gluon distribution into the parametrization of the proton structure function and its derivative with respect to $\ln Q^2$ in s -space in Eq.(16) is given by the following form

$$\begin{aligned}g^{(\varphi)}(s, Q^2) &= k^{(\varphi)}(a_s(Q^2), s) Df_2(s, Q^2) \\ &\quad - h^{(\varphi)}(a_s(Q^2), s) f_2(s, Q^2),\end{aligned}\quad (17)$$

where

$$\begin{aligned}Df_2(s, Q^2) &= \partial f_2(s, Q^2) / \partial \ln Q^2, \\ k^{(\varphi)}(a_s(Q^2), s) &= 1 / (< e^2 > \Theta_f^{(\varphi)}(a_s(Q^2), s)), \\ h^{(\varphi)}(a_s(Q^2), s) &= \Phi_f^{(\varphi)}(a_s(Q^2), s) k^{(\varphi)}(a_s(Q^2), s).\end{aligned}$$

The coefficient functions Φ_f and Θ_f in the Laplace space s are given by:

- at LO approximation

$$\begin{aligned}\Theta_f^{(0)}(a_s, s) &= 2n_f a_s(Q^2) \left[\frac{1}{1+s} - \frac{2}{2+s} + \frac{2}{3+s} \right], \quad (18) \\ \Phi_f^{(0)}(a_s, s) &= a_s(Q^2) \left[4 - \frac{8}{3} \left(\frac{1}{1+s} + \frac{1}{2+s} + 2S_1(s) \right) \right],\end{aligned}$$

Here $S_1(s) = \psi(s+1) + \gamma_E$, where $\psi(x)$ is the digamma function and $\gamma_E = 0.5772156\dots$ is Euler constant.

The explicit expressions for the NLO and NNLO kernels in s space are rather cumbersome; therefore, we recall that we are interested in investigation of the kernels in small x [30,31], as

- at NLO approximation

$$\begin{aligned}\Theta_f^{(1)}(a_s, s) &\simeq \Theta_f^{(0)}(s) + a_s^2(Q^2) C_A T_f \left[\frac{40}{9s} \right], \quad (19) \\ \Phi_f^{(1)}(a_s, s) &\simeq \Phi_f^{(0)}(s) + a_s^2(Q^2) C_F T_f \left[\frac{40}{9s} \right],\end{aligned}$$

and

- at NNLO approximation

$$\begin{aligned}\Theta_f^{(2)}(a_s, s) &\simeq \Theta_f^{(1)}(s) + a_s^3(Q^2) \left\{ n_f \left[-\frac{1268.300}{s} + \frac{896}{3s^2} \right] \right. \\ &\quad \left. + n_f^2 \left[\frac{1112}{243s} \right] \right\}, \quad (20) \\ \Phi_f^{(2)}(a_s, s) &\simeq \Phi_f^{(1)}(s) + a_s^3(Q^2) \left\{ n_f \left[-\frac{506}{s} + \frac{3584}{27s^2} \right] \right. \\ &\quad \left. + n_f^2 \left[\frac{256}{81s} \right] \right\}.\end{aligned}$$

The standard representation for QCD couplings in LO up to NNLO (within the $\overline{\text{MS}}$ -scheme) approximations are

defined by

$$\begin{aligned}\alpha_s^{\text{LO}}(t) &= \frac{4\pi}{\beta_0 t}, \\ \alpha_s^{\text{NLO}}(t) &= \frac{4\pi}{\beta_0 t} \left[1 - \frac{\beta_1}{\beta_0^2} \frac{\ln t}{t} \right], \\ \alpha_s^{\text{NNLO}}(t) &= \frac{4\pi}{\beta_0 t} \left[1 - \frac{\beta_1}{\beta_0^2} \frac{\ln t}{t} \right. \\ &\quad \left. + \frac{1}{\beta_0^3 t^2} \left\{ \frac{\beta_1^2}{\beta_0} (\ln^2 t - \ln t - 1) + \beta_2 \right\} \right],\end{aligned}$$

where β_0 , β_1 and β_2 are the one, two and three loop correction to the QCD β -function and $t = \ln \frac{Q^2}{\Lambda^2}$, Λ is the QCD cut-off parameter.

Now the inverse Laplace transforms of Eq.(17) can be easily performed by the following form as

$$\begin{aligned}\widehat{\mathcal{G}}^{(\varphi)}(v, Q^2) &\equiv \mathcal{L}^{-1}[g^{(\varphi)}(s, Q^2)(s, Q^2); v] \\ &= \mathcal{L}^{-1}[k^{(\varphi)}(a_s(Q^2), s) Df_2(s, Q^2) \\ &\quad - h^{(\varphi)}(a_s(Q^2), s) f_2(s, Q^2); v],\end{aligned}\quad (21)$$

where the inverse transform of a product to the convolution of the original functions, giving [32]

$$\mathcal{L}^{-1}[f(s) \times h(s); v] = \int_0^v \widehat{F}(w) \widehat{H}(v-w) dw.$$

The result for the color dipole cross section at scale μ^2 is

$$\sigma_{\text{dip}}^{(\varphi)} = \sigma_0 \left\{ 1 - \exp\left(-\frac{\pi^2 r^2 \alpha_s(\mu^2) G^{(\varphi)}(\tilde{x}, \mu^2)}{3\sigma_0}\right) \right\}, \quad (22)$$

where

$$\begin{aligned}G^{(\varphi)}(x, \mu^2) &= \int_x^1 \left[DF_2\left(\ln \frac{1}{y}, \mu^2\right) k^{(\varphi)}(a_s(\mu^2), \ln \frac{y}{x}) \right. \\ &\quad \left. - F_2\left(\ln \frac{1}{y}, \mu^2\right) h^{(\varphi)}(a_s(\mu^2), \ln \frac{y}{x}) \right] \frac{dy}{y}.\end{aligned}\quad (23)$$

We therefore obtained an explicit solution for the color dipole cross section $\sigma_{\text{dip}}(x, r)$ in terms of the parametrization of $F_2(x, \mu^2)$ and its derivative with respect to $\ln \mu^2$ at LO up to NNLO approximations due to the form of kernels.

3. Numerical Results

The effective parameters in the GBW model have been extracted from a fit of the HERA data according to Ref. [1]:

$$\begin{aligned}\sigma_0 &= 23 \text{ mb}, \quad \lambda = 0.288, \quad x_0/10^{-4} = 3.04, \\ C &= 0.38, \quad \mu_0^2 = 1.73 \text{ GeV}^2\end{aligned}$$

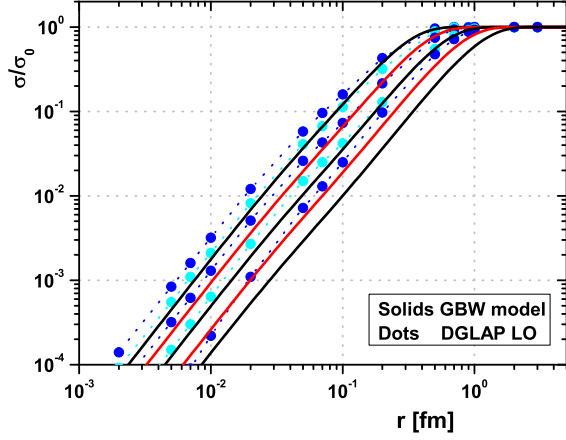


FIG. 1: The extracted ratio $\sigma_{\text{dip}}/\sigma_0$ as a function r for $x = 10^{-6}..10^{-2}$ (curves from left to right, respectively) from the parameterization of F_2 within the LO approximation (circle-dot curves), Eq.(22), compared with the GBW model (solid curves), Eq.(3).

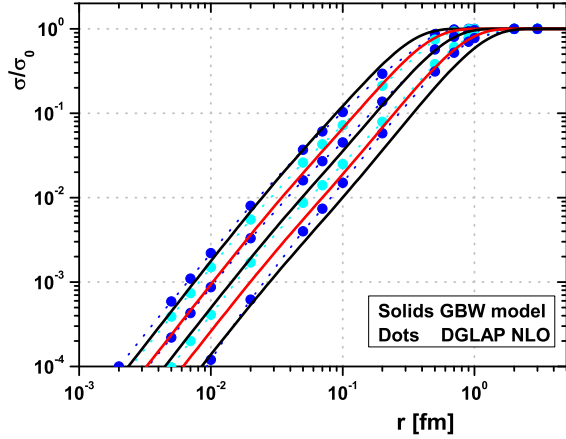


FIG. 2: The same as Fig.1 within the NLO approximation.

We have calculated the r -dependence, at low x , of the ratio $\sigma_{\text{dip}}/\sigma_0$ (i.e., Eq.(22)) in the LO up to NNLO, approximations. Results of calculations and comparison with the GBW model [1] are presented in Figs.1-3, where the circle-dot lines correspond to the extracted $\sigma_{\text{dip}}/\sigma_0$ in the LO up to NNLO approximations, respectively.

Calculations have been performed at the Bjorken variable x to vary in the interval $x = 10^{-6}..10^{-2}$. The DGLAP improved model due to the parameterization of $F_2(x, Q^2)$ giving a good description of the ratio $\sigma_{\text{dip}}/\sigma_0$ in comparison with the GBW saturation model at low x

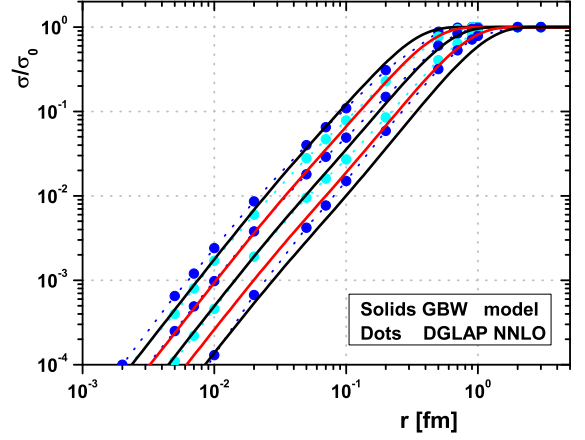


FIG. 3: The same as Fig.1 within the NNLO approximation.

in a wide range of the momentum transfer Q^2 . Figures 1-3 clearly demonstrates that the extraction procedure provides correct behaviors of the extracted $\sigma_{\text{dip}}/\sigma_0$ within the LO up to NNLO approximations. At low and high Q^2 the extracted values of $\sigma_{\text{dip}}/\sigma_0$ are in a good agreement with the GBW saturation model. We observe that the NNLO corrections are in a very good agreement with the GBW model in comparison with the LO and NLO corrections in a wide range of r . We see that the two results (the GBW and DGLAP improved models) overlap in small and large values of r , where the gluon distribution obtained from the parametrization of the proton structure function plays a significant role in the evolution of the gluon distribution.

A particular interests present the ratio $\sigma_{\text{dip}}/\sigma_0$ defined by the scaling variable rQ_s where all the curves in the GBW model merge into one solid line. In Figs.4-6 we have shown that the ratio $\sigma_{\text{dip}}(x, r)/\sigma_0$ has a property of geometric scaling as $\sigma_{\text{dip}}(x, r) = \sigma_{\text{dip}}(rQ_s(x))$. The results of the DGLAP improved saturation model due to the parametrization of the proton structure function have become a function of a single variable, rQ_s , for all values of r and x at LO up to NNLO approximations in figures 1-3 respectively. From Figure 6 one can infer that the NNLO results essentially improve the agreement with the geometric scaling in the GBW model in comparison with the LO and NLO calculations. The geometric scaling in the dipole cross sections in these calculations is visible in a wide range of rQ_s at LO up to NNLO approximations. In these figures we observe that the violation between the geometric scaling of our results and GBW model for low rQ_s is clearly visible. In this region, the violations are rather small and can be covered by the statistical errors in the parametrization of the proton structure function and its derivative. In Fig.7, the

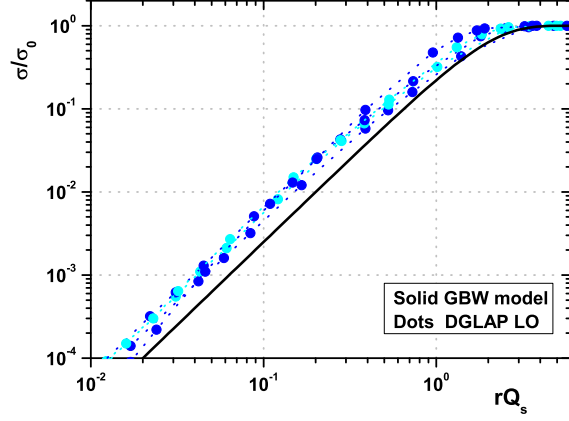


FIG. 4: The extracted ratio $\sigma_{\text{dip}}(rQ_s(x))/\sigma_0$ as a function rQ_s for $x = 10^{-6}..10^{-2}$ from the parameterization of F_2 within the LO approximation (circle-dot curves) merges into one line due to the geometric scaling and compared with the GBW model (solid curve).

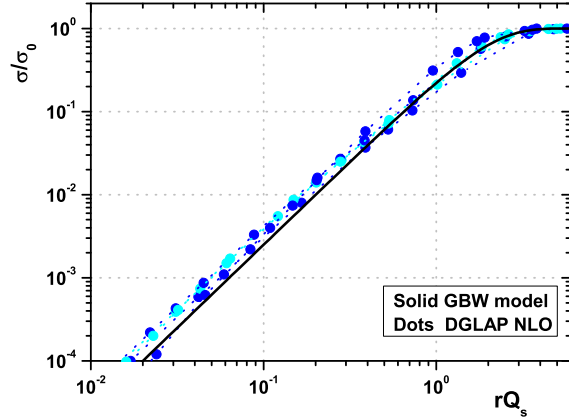


FIG. 5: The same as Fig.4 within the NLO approximation.

rQ_s dependence of the ratio $\sigma_{\text{dip}}(rQ_s(x))$ at $x = 10^{-4}$ compared with the GBW saturation model. The error bands illustrated in this figure are the statistical errors in the parametrization of F_2 and its derivative, where the fit parameter errors are shown in Table I. As can be seen from the related figures, the ratio results with respect to the Laplace transform method are consistent with the geometric scaling at low and large values of rQ_s . Summarising, the essential elements of the GBW model, the saturation scale and geometric scaling, are preserved in the DGLAP improved dipole cross section when the gluon distribution function is derivative from

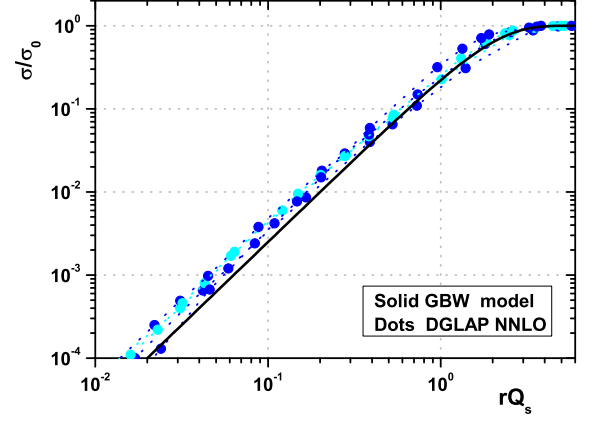


FIG. 6: The same as Fig.4 within the NNLO approximation.

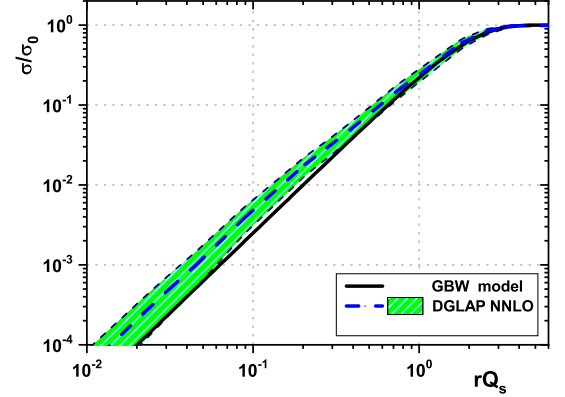


FIG. 7: The extracted ratio $\sigma_{\text{dip}}(rQ_s(x))/\sigma_0$ as a function rQ_s for $x = 10^{-4}$ within the NNLO approximation (dashed curves), accompanied with the statistical errors in the parametrization of F_2 and its derivative, compared with the GBW model (solid curve).

the parametrization of the proton structure function and its derivative due to the Laplace transforms method in a wide range of the variables r and rQ_s respectively.

4. Conclusions

In conclusion, we have presented a certain theoretical model at LO up to NNLO approximations to describe the color dipole cross section based on the Laplace transforms method at small values of x . Indeed, there are various methods to consider the color dipole model to obtain σ_{dip} , and in this paper, we have shown that

the method of the Laplace transform technique is also the reliable and alternative scheme to obtain the color dipole cross section, analytically. A detailed analysis has been performed to find an analytical solution of the color dipole cross section into the parametrization of $F_2(x, Q^2)$ and its derivative of the proton structure function with respect to $\ln Q^2$ at LO up to NNLO approximations. We used the DGLAP improved model of the dipole cross section with saturation in which the parameterization of the proton structure function is used. The results according to the saturation scale and geometric scaling are consistent with the GBW saturation model in a wide range of r and rQ_s , respectively. With considering the statistical errors due to the effective parameters, the NNLO results give a reasonable data description in comparison with the other models. Indeed, the small dipole size part of the dipole cross section is improved in comparison with the DGLAP improved model which is based on the evolution of gluon density in this region. As a summary, we have analyzed the dipole cross section at low values of x and shown that the geometric scaling holds for the DGLAP improved model if the gluon distribution is defined by the parameterization of the proton structure function and this is comparable with the GBW model curve in the whole region rQ_s .

ACKNOWLEDGMENTS

The author is grateful to Razi University for the financial support of this project and would like to thank A.M.Stasto for carefully reading the paper and for critical notes.

REFERENCES

1. K. Golec-Biernat and S.Sapeta, JHEP **03**, 102 (2018).
2. I. Abt et al., Phys. Rev. D **96**, 014001 (2017).
3. F. D. Aaron et al., [H1 and ZEUS Collaborations], JHEP **01**, 109 (2010); H. Abramowicz et al., [H1 and ZEUS Collaborations], Eur. Phys. J. C **75**, 580 (2015).
4. Yu.L.Dokshitzer, Sov.Phys.JETP **46**, 641(1977); G.Altarelli and G.Parisi, Nucl.Phys.B **126**, 298(1977); V.N.Gribov and L.N.Lipatov, Sov.J.Nucl.Phys. **15**, 438(1972).
5. V.S.Fadin, E.A.Kuraev and L.N.Lipatov, Phys.Lett.B **60**, 50(1975); L.N.Lipatov, Sov.J.Nucl.Phys. **23**, 338(1976); I.I.Balitsky and L.N.Lipatov, Sov.J.Nucl.Phys. **28**, 822(1978).
6. M.Kuroda and D.Schildknecht, Phys.Lett. B **670**, 129(2008); Phys.Rev. D **96**, 094013(2017); Int. J. Mod. Phys. A **31**, 1650157 (2016).

TABLE I: The effective Parameters at low x for $0.15 \text{ GeV}^2 < Q^2 < 3000 \text{ GeV}^2$ provided by the following values. The fixed parameters are defined by the Block-Halzen fit to the real photon-proton cross section as $M^2 = 0.753 \pm 0.068 \text{ GeV}^2$ and $\mu^2 = 2.82 \pm 0.290 \text{ GeV}^2$.

parameters	value
a_{00}	$2.550 \times 10^{-1} \pm 1.60 \times 10^{-2}$
a_{01}	$1.475 \times 10^{-1} \pm 3.025 \times 10^{-2}$
a_{10}	$8.205 \times 10^{-4} \pm 4.62 \times 10^{-4}$
a_{11}	$-5.148 \times 10^{-2} \pm 8.19 \times 10^{-3}$
a_{12}	$-4.725 \times 10^{-3} \pm 1.01 \times 10^{-3}$
a_{20}	$2.217 \times 10^{-3} \pm 1.42 \times 10^{-4}$
a_{21}	$1.244 \times 10^{-2} \pm 8.56 \times 10^{-4}$
a_{22}	$5.958 \times 10^{-4} \pm 2.32 \times 10^{-4}$
n	11.49 ± 0.99
λ	2.430 ± 0.153
$\chi^2(\text{goodness of fit})$	0.95

7. Amir H.Rezaeian and I.Schmidt, Phys.Rev. D **88**, 074016 (2013).
8. K.Golec-Biernat and M.Wüsthoff, Phys. Rev. D **59**, 014017 (1999); Phys. Rev. D **60**, 114023 (1999).
9. E.Iancu,K.Itakura and S.Munier, Phys.Lett.B **590**, 199 (2004).
10. J.Bartels, K.Golec-Biernat and H.Kowalski, Phys. Rev. D **66**, 014001 (2002); Acta Phys.Polon.B **33**, 2853 (2002).
11. J.R.Forshaw and G.Shaw, JHEP **12**, 052 (2004).
12. K.Golec-Biernat, J.Phys.G **28**, 1057 (2002); Acta Phys.Polon.B **33**, 2771 (2002).
13. H.Kowalski and D.Teaney, Phys. Rev. D **68**, 114005 (2003).
14. G. Soyez, arXiv: 0705.3672 (2007); M.V.T. Machado, arXiv: 0512264 (2006); J. T. de Santana Amaral et al., arXiv:0612091 (2006).
15. B. Ducloue et al., arXiv:1912.09196 (2019).
16. K.Golec-Biernat and S. Sapeta, Phys. Rev. D **74**, 054032 (2006).
17. I. Balitsky, Nucl. Phys. B **463**, 99 (1996); Y. V. Kovchegov, Phys. Rev. D **60**, 034008(1999); Phys. Rev. D **61**, 074018 (2000).
18. A.M.Stasto, K.Golec-Biernat and J.Kwiecinski, Phys.Rev.Lett. **86**, 596 (2001).
19. E. Iancu and R. Venugopalan, arXiv:hep-ph/0303204.
20. Y.S.Jeong, C.S.Kim, M.V.Luu and M.H.Reno, JHEP **11**, 025 (2014).
21. Z.Jalilian and G.R.Boroun, Phys.Lett.B **773**, 455 (2017); Z.Jalilian and G.R.Boroun, Chin.Phys.C **45**,

- 023101 (2020); B.Rezaei and G.R.Boroun, Phys.Rev.C **101**, 045202 (2020).
22. G.R.Boroun and B.Rezaei, Nucl.Phys.A **990**, 244 (2019); G.R.Boroun, Eur.Phys.J.A **57**, 219 (2021); G.R.Boroun and B.Rezaei, Phys.Rev.C **103**, 065202 (2021).
23. L.P.Kaptari, A.V.Kotikov, N.Yu.Chernikova, and P.Zhang, Phys.Rev.D **99**, 096019 (2019).
24. G.R.Boroun and B.Rezaei, Phys.Rev.D **105**, 034002 (2022).
25. M. M. Block, L. Durand and P. Ha, Phys. Rev.D **89**, no. 9, 094027 (2014).
26. M. Froissart, Phys. Rev. **123**, 1053 (1961).
27. F.D. Aaron et al., [H1 and ZEUS Collaborations], JHEP **1001**, 109 (2010).
28. J. Blumlein, V. Ravindran and W. van Neerven, Nucl. Phys. B **586**, 349(2000); S.Catani and F.Hautmann, Nucl.Phys.B**427**, 475(1994).
29. D.I.Kazakov and A.V.Kotikov, Phys.Lett.B**291**, 171(1992); E.B.Zijlstra and W.L.van Neerven, Nucl.Phys.B383, 525(1992).
30. A. Vogt, S. Moch and J.A.M. Vermaseren, Nucl.Phys.B **691**, 129 (2004).
31. W.L. van Neerven and A.Vogt, Phys.Lett.B **490**, 111 (2000).
32. M.M. Block, L. Durand, and D.W. McKay, Phys. Rev. D **79**, 014031 (2009).